IOP PUBLISHING PHYSICS IN MEDICINE AND BIOLOGY

Phys. Med. Biol. **54** (2009) 4927–4943 doi:10.1088/0031-9155/54/16/006

In vivo imaging of irreversible electroporation by means of electrical impedance tomography

Yair Granot[1,4,5], Antoni Ivorra[2,5], Elad Maor[1] and Boris Rubinsky[1,2,3]

[1] Biophysics Graduate Group, University of California at Berkeley, Berkeley, CA 94720, USA
[2] Departments of Mechanical Engineering and Bioengineering, University of California at Berkeley, Berkeley, CA 94720, USA
[3] Center for Bioengineering in the Service of Humanity and Society, School of Computer Science and Engineering, Hebrew University of Jerusalem, Givat Ram, Jerusalem 91904, Israel

E-mail: yair.granot@gmail.com

Received 4 March 2009, in final form 29 June 2009
Published 30 July 2009
Online at stacks.iop.org/PMB/54/4927

Abstract

Electroporation, the increased permeability of cell membranes due to a large transmembrane voltage, is an important clinical tool. Both reversible and irreversible *in vivo* electroporation are used for clinical applications such as gene therapy and solid malignant tumor ablation, respectively. The primary advantage of *in vivo* electroporation is the ability to treat tissue in a local and minimally invasive fashion. The drawback is the current lack of control over the process. This paper is the first report of a new method for real-time three-dimensional imaging of an *in vivo* electroporation process. Using two needle electrodes for irreversible electroporation and a set of electrodes for reconstructing electrical impedance tomography (EIT) images of the treated tissue, we were able to demonstrate electroporation imaging in rodent livers. Histology analysis shows good correlation between the extent of tissue damage caused by irreversible electroporation and the EIT images. This new method may lead the way to real-time control over genetic treatment of diseases in tissue and tissue ablation.

(Some figures in this article are in colour only in the electronic version)

1. Introduction

Electroporation is the biophysical process in which the cell membrane increases its permeability upon exposure to short (microsecond to millisecond) high electric field pulses (Chen *et al* 2008). Reversible electroporation occurs when the cell membrane is temporarily

[4] Author to whom any correspondence should be addressed.
[5] These authors contributed equally to this work

permeabilized and is commonly used for gene therapy or drug delivery. Irreversible electroporation occurs when the cell membrane permeabilization is of such a nature as to induce cell death. Electroporation is induced in tissue through a set of electrodes and until now was used without real-time control. In this study, we introduce a new method for real-time control of electroporation through electrical impedance tomography (EIT). As a case study we focus on irreversible electroporation, although the method is generally applicable to any electroporation protocol.

Irreversible electroporation is becoming an important new clinical tool for *in vivo* tissue ablation (Esser *et al* 2007, Rubinsky 2007, Maor *et al* 2008). Although the exact mechanism of electroporation, reversible as well as irreversible, is not completely understood, it is widely accepted that cell death occurs as a result of permanent damage to the cell membrane or the loss of homeostasis following a long period of high membrane permeability (Weaver and Chizmadzhev 2007). Some of the advantages of irreversible electroporation (IRE) emanate from this elegant and relatively physiologic nature of cell death, which does not alter the extracellular matrix and does not cause protein denaturation or other side effects that are often associated with necrotic tissue ablation. Furthermore, the application of short electrical pulses for IRE has little effect on the temperature of the treated tissue (Davalos *et al* 2005) and consequently this technique can be efficiently implemented even in the proximity of large blood vessels (Edd *et al* 2006, Rubinsky *et al* 2007). Clinical implementations of IRE could greatly benefit from a method to monitor and control the procedure in real time.

For a given tissue, the main parameters that determine the effect of the electric field pulses are the magnitude of the applied electric field, the number of pulses, the duration of each pulse and the pulse repetition rate (Gehl and Mir 1999, Canatella *et al* 2001, Pucihar *et al* 2002). For more than 10 years, researchers have been employing numerical methods for computing the electric field magnitude distribution and the resulting tissue volume that will be effectively electroporated under a particular sample and electrode configuration (Miklavcic *et al* 1998). However, this sort of modeling is based on some *a priori* information about the passive electrical properties of the involved tissues and on some oversimplifications of the geometry of the problem. More accurate predictions require complete knowledge of the electrical properties of the treated tissue and its surroundings, as well as the nature of the interaction between the tissue and the electrodes. This is not feasible with the current technology and an alternative method, using an iterative protocol, is preferable. By monitoring the effects of electroporation pulses as they are applied, it would be possible to adjust the protocol parameters in real time so that the required results would be obtained.

As a possible real-time monitoring method, we explore in this paper the use of EIT for imaging the electroporated tissue. The fundamental hypothesis of this study is that electroporation and the consequent permeabilization of the cell membrane will cause a change in the electrical properties of the tissue and therefore yield a change in the electrical impedance tomography image.

We have previously suggested using the changes in conductivity of the electroporated tissue as a means of monitoring the extent of electroporation (Davalos *et al* 2002, 2004, Granot and Rubinsky 2007). Other methods for controlling electroporation have been proposed, such as measuring the voltage and current of the pulses (Cukjati *et al* 2007) but these were aimed at changing the pulse parameters during the pulse and may not always be efficient in estimating the efficacy of the entire electroporation process.

In an EIT implementation, electrodes are placed around the tissue and very small currents are injected into the tissue while the voltage on the tissue boundary is measured (Jossinet *et al* 2002). Using the finite elements method, the impedance of the entire tissue is modeled, and a solution for the most likely configuration that fits the problem is obtained (Lionheart

2004). In this paper, we describe our 3D EIT implementation that was based on the EIDORS suite (Adler and Lionheart 2006) and was used to image the changes in electroporated rodent hepatic tissue.

At present, electrical impedance tomography is generally considered a poor method for general medical imaging because it yields blurry images when compared with other modalities for stationary imaging (Patterson 2005). On the other hand, EIT involves low cost equipment and does not require potentially dangerous radiations. More importantly, EIT is a suitable technique for imaging fast dynamic phenomena (Metherall *et al* 1996, Bayford 2006). To the best of our knowledge, EIT is the only imaging technique that is based on a measurement principle (measuring the passive electrical properties of tissues) that is directly influenced by the electroporation phenomenon. Therefore, EIT may be the only feasible candidate for imaging electroporation with feedback control purposes. Other techniques may be able to detect the indirect consequences of electroporation but, because of their indirect measurement process, these alternative methods may be too slow for a feedback scheme. For instance, it has been discovered that IRE induces hypoechoic areas in sonography several tens of seconds after the application of the pulses (Lee *et al* 2007, Rubinsky *et al* 2007).

2. Methods

In each animal (Sprague-Dawley rats) employed in this study (15), a sequence of high voltage pulses (eight pulses of 100 μs with an inter-pulse interval of 500 ms) is applied to the surgically exposed liver through a pair of needle electrodes. Immediately after each pulse (<200 ms), by means of two multi-electrode plates clamping the liver and a custom-developed electronic setup, multiple impedance measurements are taken. These measurements are processed using EIT reconstruction algorithms and images of the changes in tissue conductivity due to electroporation are obtained. Later, these images are compared to actual histological analysis of the treated livers. The whole methodology is described in detail in the following sections.

The specific electroporation protocol used here (eight pulses of 100 μs) was chosen because it is employed by most researchers within the *in vivo* electroporation field (Mir *et al* 1991, Hofmann 2000). The application of multiple short pulses is more efficient, in terms of cell membrane permeabilization, than the application of a single long pulse and minimizes tissue heating due to the Joule effect.

2.1. Hardware system overview

The electronic instrumentation system employed here (figure 1) can be conceptually divided into two subsystems: (1) an electroporation subsystem and (2) a 64-electrode EIT subsystem. An automated switching mechanism protected the system from a case in which high voltage pulses were delivered to the tissue while the EIT subsystem was simultaneously connected to the tissue through the EIT electrodes. Such conditions would not only produce unpredictable measurements, because of saturation of different electronic parts, but may also lead to irreversible damage to these parts.

The electroporation protocol in all the experiments reported here consisted of eight square pulses of 100 μs with an interval of 500 ms between pulses; only the voltage magnitude was modified between experiments. After each pulse, the EIT subsystem recorded the required measurements for a single EIT image. This acquisition process started 20 ms after the detection of the electroporation pulse and lasted 154 ms.

The high voltage pulse generator was a commercial unit (ECM 830, Harvard Apparatus, Holliston, MA). Electroporation current and voltage waveforms were recorded using

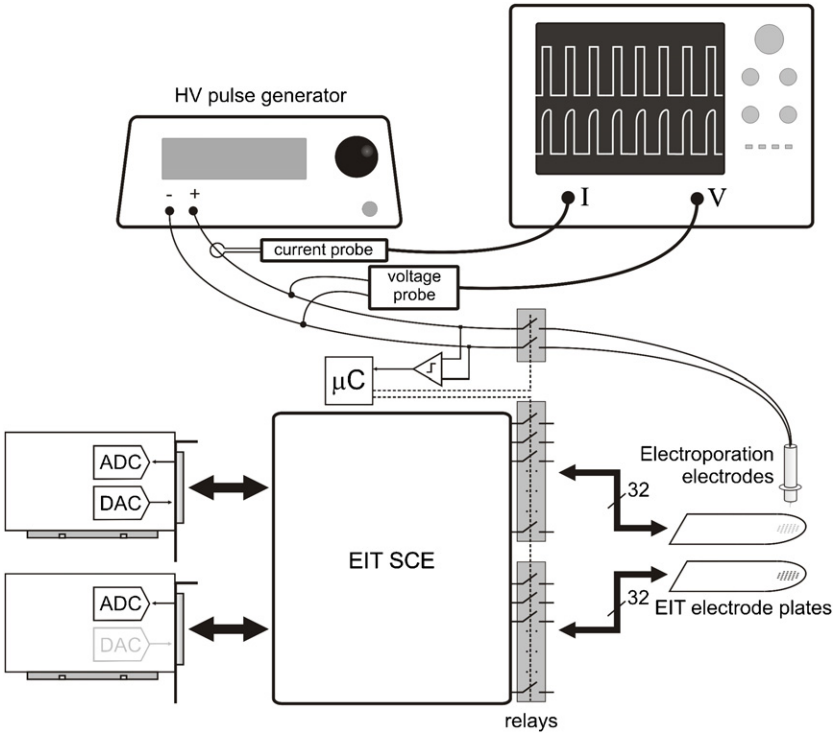

Figure 1. General architecture of the electronic instrumentation system. The high voltage (HV) pulse generator delivers its pulses to the bipolar electroporation probe (electroporation electrodes) through a relay that is controlled by a microcontroller (μC). The applied voltage and current are monitored with special probes and a digital scope. The microcontroller also controls a bank of relays that connects the EIT electrodes to the EIT measurement system. The EIT measurement system consists of some signal conditioning electronics (SCE) and two commercial data acquisition boards.

high-performance oscilloscope probes (current probe AP015 and high voltage probe ADP305 from LeCroy Corp., Chestnut Ridge, NY). Both signals were captured with a digital oscilloscope (WaveRunner 44Xi, LeCroy Corp.) in a segmented memory mode.

The EIT measurement subsystem can be described as a four-electrode system able to address 64 electrodes. Current (5 kHz, 250 μA_{RMS}) is injected between two electrodes selected by analogue switches and voltage differences are picked up simultaneously from a set of electrode pairs (configurable by hardwiring). In the configuration employed here, for each image, 32 electrode pairs were sequentially selected for current injection (4.8 ms per pair) and voltage differences were measured from 32 electrode pairs. That is, the total number of measurements per image was 1024. These measurements contain magnitude and phase angle data. However, in the current study we only employed phase angle information to determine the sign of voltage value.

2.2. Electrode setup

The EIT electrode setup (figure 2) was implemented by standard printed circuit board (PCB) fabrication techniques. It consisted of 64 gold-coated electrodes (1 mm squares separated

by 1 mm) etched on two 1.6 mm thick PCBs (manufactured by Sierra Proto Express Inc., Sunnyvale, CA). Each array (32 electrodes) was designed to face the other one across a lobe of the liver at a distance prescribed by a spacer. In order to improve the four-electrode impedance measurements performed in EIT data acquisition, the electrode–tissue interface impedance was reduced via electrochemical deposition of platinum on the gold electrodes (Geddes 1972). The electroplating solution consisted of 7.5 ml of distilled water, 0.25 g of Cl_4Pt, 3 mg of $Pb(CH_3COO) \cdot 3H_2O$ and 2.5 ml of HCl (0.1 M). The electrodes (cathodes) were individually plated connecting them to a +15 V voltage source through a 3.5 kΩ resistor, resulting in a current of about 3.5 mA. A 2×2 cm^2 silver foil was employed as anode. Each EIT electrode was plated individually for 35 s divided into 5 s cycles. After this process, the magnitude of the electrode interface impedance in physiological solution (NaCl 0.9%) was well below 2×10^{-4} Ω m^2 at 1 kHz.

The electroporation electrodes consisted of two stainless steel needles (diameter = 0.4 mm) that were inserted into the tissue through the upper PCB down to 1.7 mm (distance from the needle tip to the EIT electrode plate).

2.3. Further details on the EIT system

The EIT hardware follows a classical architecture (figure 3) in which a single bipolar current source is sequentially switched between different electrode pairs and a set of differential voltages is obtained simultaneously from other electrode pairs (Saulnier 2005). Physically, it consisted of two custom-made PCBs (168×186 mm^2) and two commercial multifunction acquisition boards (NI PCI-6071E, National Instruments Corp., Austin, TX).

The bipolar current was generated from a sinusoidal voltage signal by means of the so-called Howland circuit (Bertemes-Filho *et al* 2000) where the original voltage signal fed to the voltage-to-current converter was synthesized by a 12 bit digital-to-analogue converter working at 800 k Samples s^{-1} on the acquisition board (DAQ board). A low-pass filter (two-stage Sallen-Key Low Pass filter with a 1 MHz cutoff frequency; fourth order) was intercalated in order to remove the high frequency contents of the synthesized signal. For all the experiments described here, we chose the maximum amplitude voltage provided by the acquisition board (10 V_{peak}) and such voltage amplitude translates to an output current amplitude of 350 μA_{peak} (∼250 μA_{RMS}).

Then the bipolar current was relayed to the electrode pair selected by the microcontroller (PIC16F877, Microchip Technology, Chandler, AZ) by means of a combination of 16-channel analogue multiplexers (MAX336, Maxim Integrated Products, Sunnyvale, CA). The sequence of electrode pairs for current injection, known as 'current pattern', was specified in the internal program memory of the microcontroller. Each electrode pair was active for 24 cycles of the 5 kHz signal (4.8 ms). The first eight cycles were reserved for switching settling and in order to allow the system to reach the permanent regime. The remaining cycles were used to extract the measurement. Voltage measurements were obtained from the samples acquired by the 12 bit analogue-to-digital converter of the DAQ board operating at 50 kSamples s^{-1} per channel.

Post-acquisition processing consisted of obtaining the real and imaginary parts of each signal in accordance to the generated signal for the current. This was done by a digital version of the quadrature demodulator (Roberts 2004).

The whole acquisition process was governed by custom-developed routines in a LabVIEW environment (LabVIEW 8.5 by National Instruments, Corp., Austin, TX; Windows XP by Microsoft Corp., Redmond, WA; OptiPlex Pentium 4 by Dell Corp., Round Rock, TX). Post-acquisition processing was performed in MATLAB version 7 (The Matworks, Inc., Natick, MA).

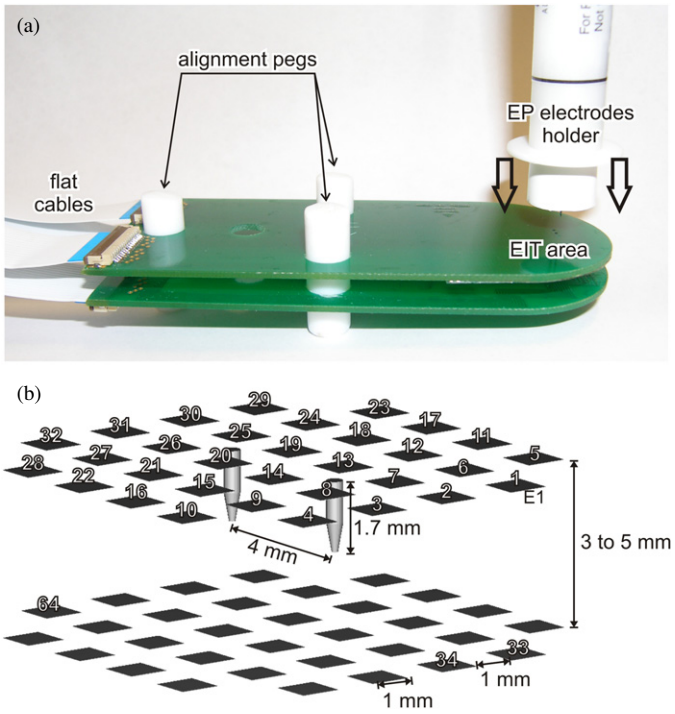

Figure 2. (a) Picture of the EIT electrode plates. The holder for the electroporation (EP) electrodes is shown above the plates; the needles are barely visible. The EIT electrodes are not visible. (b) Representation of the EIT electrodes and the electroporation needles.

An important parameter of any measurement system is its signal-to-noise ratio, which may be defined in several fashions. If no electroporation is performed, consecutive image acquisitions should imply identical measurements except for the errors caused by noise and interferences. In particular, for each electrode pair the set of 32 voltages obtained for each consecutive acquisition should be identical. Hence from this fact, it is possible to define a signal-to-noise ratio of the overall EIT system (Wilson *et al* 2001): for each current combination, the signal-to-noise ratio is the ratio of the mean to the standard deviation for a contiguous sequence of demodulated measurements. According to this definition, the system employed here had a signal-to-noise ratio of 42 dB when continuous measurements were taken in *in vivo* rat liver.

2.4. In vivo procedure

Fifteen male Sprague-Dawley rats weighting 275–325 g were used in this study. All animals received humane care from a properly trained professional in compliance with both the Principals of Laboratory Animal Care and the Guide for the Care and Use of Laboratory Animals, published by the National Institute of Health (NIH publication no. 85–23, revised 1985). Animals were anaesthetized throughout the procedure and core body temperature was maintained using a temperature controller (TCAT-2, Harvard Apparatus, Holliston, MA).

The lower ventral lobe of the liver was exposed and placed between the two electrode plates. Spacers were used to keep the two plates 3 mm apart in rats 1 through 13 and 4.5 mm in rats 14 and 15.

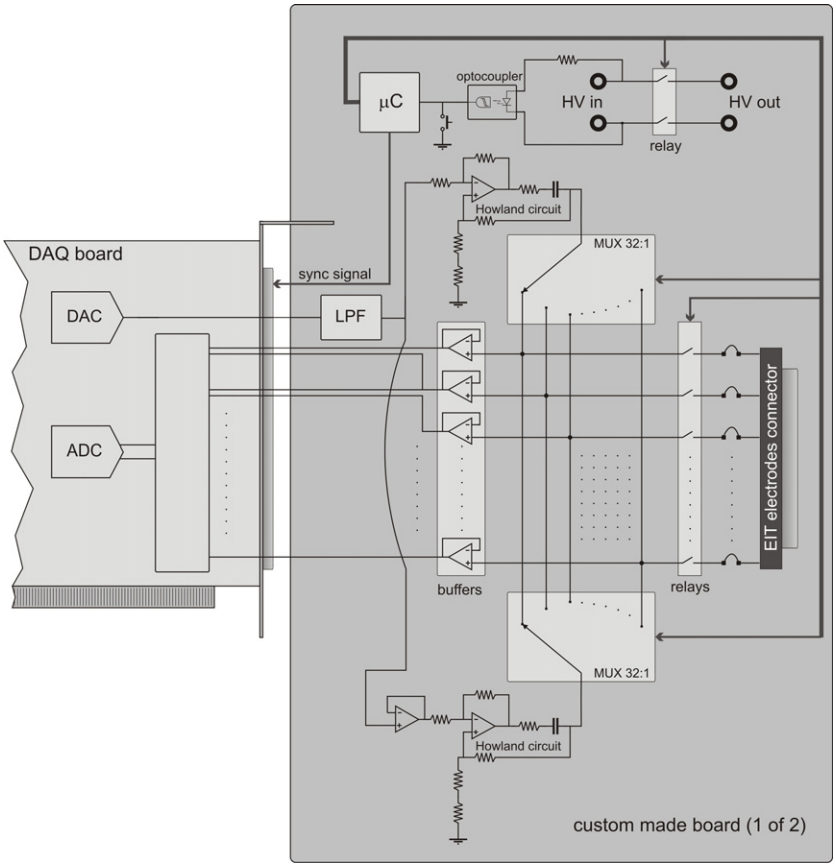

Figure 3. Architecture of the EIT subsystem (only one board out of two is represented). Acquisition is triggered manually (push-button) or automatically when a high voltage pulse is detected through an optocoupler. The whole measurement process is controlled by a programmable microcontroller (μC). See text.

An initial EIT measurement was taken before introducing the electroporation electrodes. Next, a reference measurement was taken with the electrodes in place. Then we applied eight pulses as described above (EIT measurements are automatically triggered at the end of each pulse). After the last electroporation pulse, six additional manually triggered EIT measurements were taken at 10, 20, 30, 60 120 and 180 s.

The electroporation electric field is not homogeneous for the electrode configuration employed here. Some tissue regions experience a high electric field that may result in IRE while others may go through reversible electroporation or not experience any effect at all. In the two-needle configuration used in these experiments, the highest field is in the volume around and between the electrodes, as can be seen in figure 4 which depicts the electric field in a cross section of the tissue. Other graphical illustrations of the electric field distribution can be found in Edd and Davalos (2007). Based on finite element simulations (Granot and Rubinsky 2007) assuming a homogenous tissue as the initial condition and published electroporation thresholds (Ivorra and Rubinsky 2007), we experimented with three different voltages for the same eight-pulse electroporation protocol described above (eight pulses of

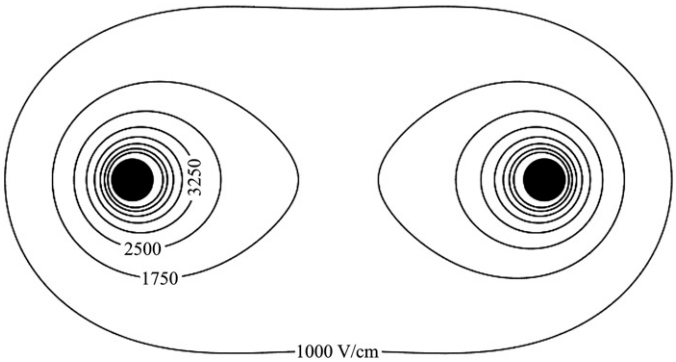

Figure 4. Cross-section representation of the electric field magnitude in the region around the needles for a 1000 V voltage difference. This simulated field distribution was obtained using a finite element method tool (COMSOL Multiphysics 3.3) following a procedure equivalent to that described in Edd and Davalos (2007).

100 μs duration with an interval of 500 ms) and the same electroporation probe (described in section 2.2).

- 1000 V: this voltage is expected to create an electric field large enough to obtain IRE ablation in a continuous region between the electrodes; this setup was selected for eight rats (labeled as 1, 4, 5, 6, 12, 13, 14 and 15).
- 500 V: this voltage is expected to result in localized IRE ablation mostly around the electrodes; this setup was selected for three rats (7, 8 and 9).
- 200 V: this voltage is expected to result in reversible electroporation near the electrodes and no effect at all in other parts of the tissue; the amount of permanent damage from this field is expected to be small; this setup was selected for two rats (10 and 11).

Following the last EIT measurement, all electrodes were removed and skin incision was sutured. Animals were kept alive for a followup period of 2 h, after which they were euthanized with an overdose of phenobarbital followed by bilateral chest dissection. The arterial tree was perfused with normal saline followed by 10% buffered formalin, and electroporated liver lobes were extracted.

2.5. Histology analysis

Electroporated lesions were cut along the plane of the needle electrodes. Slices from both sides of the needle electrodes' plane, along with a third slice of normal hepatic tissue, were fixated with 10% buffered formalin, embedded in paraffin and sectioned with a microtome (5 μm thick). One section was stained with hematoxylin and eosin (H&E). H&E stains basophilic structures in blue and eosinophilic structures in pink. It was used to demonstrate changes in the microscopic anatomy of the treated areas and to delineate those areas from the unaffected ones. Another section was used for detecting red blood cells using diaminobenzidine (DAB). The presence of red blood cells is indicative of damaged tissue. DAB undergoes an oxidation reaction, catalyzed by the heme groups in hemoglobin, in the presence of hydrogen peroxide, which produces the dark brown color reaction. Since red blood cells contain large amounts of hemoglobin, a strongly visible brown color is obtained when DAB reacts with blood. Each slide was photographed under magnification, and the damaged areas were photographed and compared with EIT results.

2.6. EIT reconstruction

Each EIT measurement included 32 current patterns, all of them injecting currents between two electrodes on the same plate. Voltage measurements were taken between pairs of electrodes which are directly across. The two measurements that included a current carrying electrode were discarded from the reconstruction process. The electroporation electrodes were not used in the EIT measurement in this case.

The reconstruction algorithm was implemented in Matlab using the finite element method and based on the EIDORS suite (Polydorides and Lionheart 2002). The basic mesh of the finite elements was constructed using COMSOL Multiphysics version 3.3[6] and had roughly 10 000 elements covering a volume of $18 \times 18 \times 5$ mm^3. The mesh elements were of varying sizes, which is the common scenario for finite element solutions. Close to the boundary and the electrodes, where the electric potential, for example, may change rapidly, the elements are relatively small. In other parts of the tissue, the elements are larger. The smaller elements are necessary to allow an accurate solution of the finite element equations, but this does not mean that the EIT image resolution will correspond to the element size. The image resolution depends on several parameters such as the current patterns, the location and the number of the electrodes and the regularization matrix (Adler and Lionheart 2006). To ensure the mathematical stability of the EIT solution, we have tried several mesh sizes and verified that their solutions converge, i.e. the solution of two different meshes for the same set of measurements produced similar results.

In our analysis we focused on the volume between the EIT electrode plates, called the region of interest (ROI) which was $12 \times 12 \times 5$ mm^3 since the electrodes cover an area slightly smaller than an 11×11 mm^2 square. The larger mesh, which spans 3 mm further than the ROI in each direction to cover the above-mentioned 18×18 mm^2 area, was important in order to ensure that currents that may have been flowing outside the electroporated area were considered during the reconstruction. The size of the mesh in terms of the Z-axis was adjusted later according to the actual thickness of the rat liver lobe that was examined so that the actual meshes that were used were either $18 \times 18 \times 4.5$ mm^3 or $18 \times 18 \times 3$ mm^3.

For the reconstruction, a time-difference imaging technique was used comparing the images to a reference value taken just before the first electroporation pulse. The reference frame was subtracted from the image frame and divided by the mean value of the reference frame, so that the total conductivity change was given in terms of the ratio of the change to the reference frame. In order to display different cross sections, the conductivity data were transformed to a 3D grid consisting of $49 \times 49 \times 19$ voxels which span the ROI. This grid is not to be confused with the mesh used for solving the equations and the choice of the voxel size is quite arbitrary, as long as the voxels are small enough to satisfy the image resolution of the EIT solution.

3. Results

3.1. EIT time evolution

As was hypothesized, the EIT images show that the conductivity of the regions close to the electrodes increases significantly, pulse after pulse, when the voltage is large enough to induce electroporation. Figure 5 shows an example of several images taken before, during and after the electroporation pulses in rat 1 which was subjected to 1000 V pulses. All of the EIT images throughout this paper are shown with identical parameters including geometrical scale

[6] www.comsol.com.

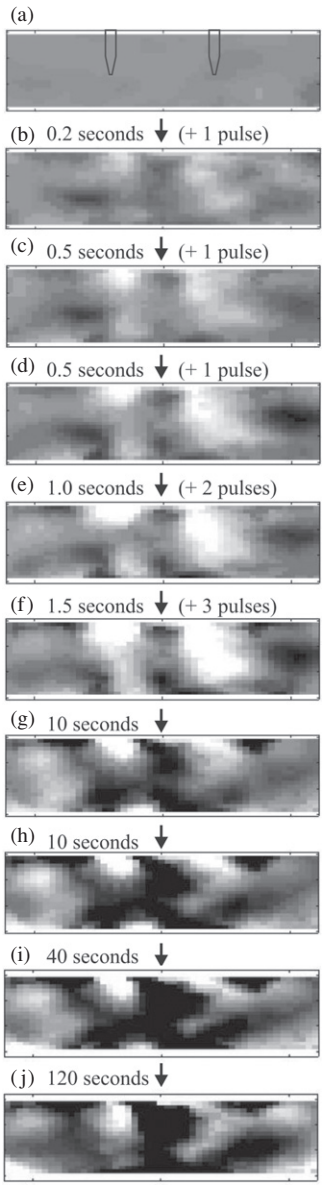

Figure 5. Time evolution of the conductivity during and after electroporation in rat 1 with a voltage of 1000 V. Brighter regions represent an increase in conductivity and darker regions represent a decrease. Central sections of 12 mm × 3 mm are displayed. (a) Before the procedure, the needle location is overlaid for the reader's convenience. (b) After the first pulse. (c) After the second pulse. (d) After the third pulse. (e) After the fifth pulse. (f) Immediately following the eighth and last pulse. (g) 10 s after the last pulse. (h) 20 s after the last pulse. (i) 60 s after the last pulse. (j) 180 s after the last pulse.

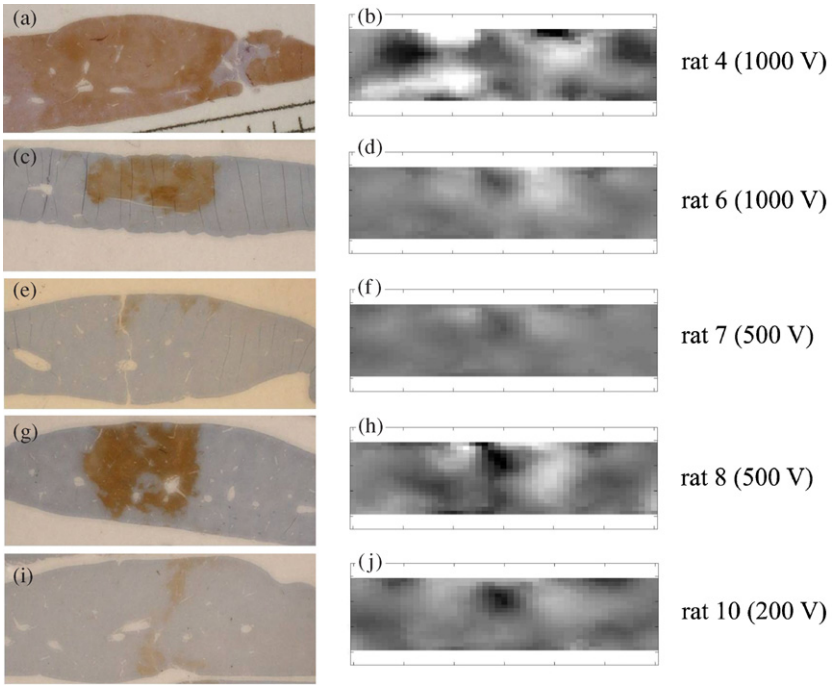

Figure 6. Some examples of histology and EIT imaging results for various voltages. Histology slides on the left column show an area of 5 mm by 12 mm. EIT images show an equivalent area of 3 mm by 12 mm. In the EIT reconstruction images, brighter regions represent an increase in conductivity and darker regions represent a decrease. (a) Histology for rat 4 (1000 V). (b) Reconstructed image for rat 4 immediately after the last pulse. (c) Histology for rat 6 (1000 V). (d) Reconstructed image for rat 6 immediately after the last pulse. (e) Histology for rat 7 (500 V). (f) Reconstructed image for rat 7 immediately after the last pulse. (g) Histology for rat 8 (500 V). (h) Reconstructed image for rat 8 immediately after the last pulse. (i) Histology for rat 10 (200 V). (j) Reconstructed image for rat 10 immediately after the last pulse.

and gray level scale. Before the procedure, the conductivity is similar to that of the reference frame and thus the image is completely gray. After a single pulse, a higher conductivity region around the area where the electroporation electrodes are located begins to appear. This region becomes more pronounced with every pulse and it also begins to expand. The appearance of dark regions after electroporation will be justified in section 4.

3.2. Correlation between the EIT images and the actual extent of damage

Figure 6 shows the results of electroporation for rats 4, 6, 7, 8 and 10. Every row in the figure depicts the results of a different IRE procedure. The left column shows the histology with DAB staining in which the damaged regions appear dark. The right column is a reconstructed image of a cross section through the plane of the electrodes immediately after the last electroporation pulse was applied (i.e. equivalent to figure 5(f)). Brighter regions in these images represent areas of increased conductivity compared with the initial conditions that were measured before the electroporation process. The gray level scale is identical in all of the EIT images.

An important example was noticed in the three experiments of the 500 V group, rats 7 through 9. Rats 7 and 9 were very similar but in rat 8 the electroporated area was much larger

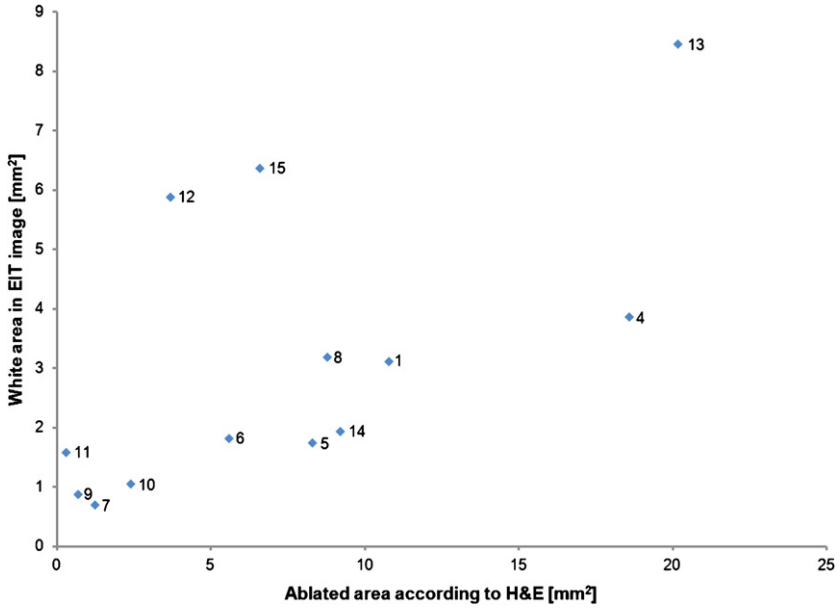

Figure 7. Correlation between the areas of ablated tissue estimated by H&E and EIT. Three of the last four experiments, which were performed with much larger rats than previous procedures, are clearly outliers. The numbers indicate the rat number. Results for rats 2 and 3 are not given due to technical difficulties during the procedure. When the outliners are rejected (12, 13 and 15), Student's *t*-test indicates that there is a significant difference ($p < 0.05$) in terms of white area between the animals with an ablated area smaller than 7.5 mm^2 and those with an ablated area larger than 7.5 mm^2 (7.5 mm^2 is the average ablated area according to H&E).

as seen in figure 6(g) which shows an almost continuous region of damaged tissue. The EIT reconstruction shows similar findings, i.e. the conductivity in the case of rat 7 has not changed very much while rat 8 has an increased conductivity around the electrodes, particularly the right electrode in figure 6(h). The significance of this disparity is discussed in section 4.

Although the exact shape of the damaged area is somewhat difficult to determine from the EIT images, there is clearly a good agreement between the extent of damage as seen in EIT and the *a posteriori* histology data. Figure 7 depicts this agreement by showing the area of the ablated region as estimated from the EIT images compared with the area of the region according to the H&E histology slides. The estimated area according to the DAB slides was very similar to that of the H&E slides. The damaged area in the EIT image was measured by counting the number of pixels which passed a conductivity threshold in the image reconstructed from measurements that were taken after the last pulse. Other criteria were also tested. Some included measuring the decreased conductivity in the 3 min data or a combination of these criteria, but all showed equivalent results. Results for rats 2 and 3 are not given due to technical difficulties during the procedure.

3.3. Influence of the EIT electrodes on the distribution of the electroporation field

It is interesting to note that the reconstructed EIT images for the 1000 V group (1, 4, 5, 6, 12, 13, 14 and 15) show two bright regions in the upper area of the cross section transversal to the electroporation needles' plane (figure 8(a)). These regions of high conductivity (i.e. high electric field magnitude) are not predicted by a simulation model in which the liver

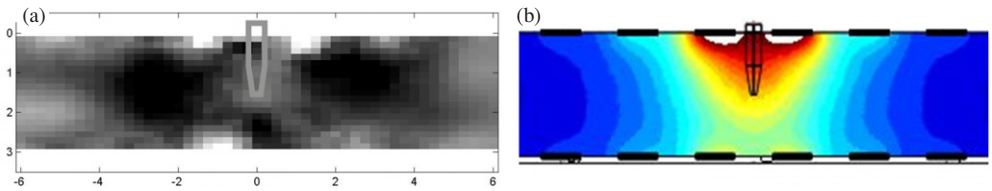

Figure 8. Cross section between the two electroporation electrodes immediately following the last electroporation pulse. (a) EIT image from rat 1; needle location is overlaid for the reader's convenience. (b) Simulated electric field with the field magnitude values above 1500 V cm^{-1} appearing in white. The simulation was carried out in COMSOL Multiphysics 3.3 with a geometrical model similar to that shown in figure 2(b) (liver slab thickness = 3 mm) and with a voltage difference of 1000 V between the needle electrodes.

is sandwiched between two dielectric planes. However, if we include in that model the conductive effect of the square EIT electrodes, two regions of high electric field magnitude appear (figure 8(b)). These regions should not be confused with the high conductivity regions near the electrode on the electrode plane shown before. The distance between these regions is smaller than the electrode distance and matches the simulated results with the effect of the EIT electrodes. This particular result stresses the ability of EIT reconstruction to identify areas of irreversible electroporation, even when these are relatively small.

The effect of the EIT electrodes on the distribution of the electroporation electric field (figure 8) can be regarded as an adverse side effect of the EIT method. Nevertheless, it must be pointed out that this effect is very localized and constrained to small regions. Furthermore, for larger tissue samples (e.g. human livers), in which the ratio of the separation distances of the electrodes to their sizes will be larger, the effect of the EIT electrodes will be substantially less significant. On the other hand, the appearance of these regions in the EIT images (figure 8(a)) is a positive result that reinforces the validity of the EIT as an imaging technology.

4. Discussion

The appearance of dark regions after electroporation deserves further discussion as it was not predicted by the main hypothesis of this paper, which are as follows: (1) high voltage pulses increase membrane permeability, (2) therefore tissue conductance increases and (3) consequently, areas close to the electrodes should look brighter than the non-affected distant areas, which should preserve their gray color. Yet the dark regions indicative of low conductance in figures 5(g)–(j) are precisely in a region between the electrodes, where the electric field during electroporation was quite intense. These results were reproducible in all of the animal experiments and could not be attributed to an error in the protocol, the measurements or the reconstruction procedure. Thus, an explanation is needed here.

Opportunely, before carrying out the present study, we performed another study in which the liver impedance of rats was monitored after electroporation (Ivorra and Rubinsky 2007). In that study, we noted that when a reversible electroporation protocol was applied, the conductivity of the tissue first increased after each pulse, but afterward it started to decrease and it dropped well below the original conductivity value within a few seconds. We believe that such a decrease in conductance may be due to a cell swelling effect: the permeabilization of the membrane by electroporation causes an osmotic influx of water (cell swelling) which narrows the extracellular ionic pathways in the tissue and, consequently, causes a decrease in the total tissue conductivity (or an increase in the impedance magnitude at low and moderate frequencies, up to 50 kHz). Such hypothesis is supported by previous studies on dense

cell suspensions (Abidor *et al* 1994, Pavlin *et al* 2005). Of particular importance is the study by Abidor *et al* where the authors show that the decrease in conductance after mild electroporation depends on the osmolarity of the extracellular solution, which indicates that 'porated cells experienced a slow colloidal-osmotic swelling'. To the best of our knowledge, such a statement has not been challenged since 1994. Furthermore, in studies which monitor tissue ischemia, another physiological phenomenon known to cause cell swelling, conductance has also decreased at low and moderate frequencies (Rigaud *et al* 1996).

So, in terms of changes in electrical conductivity, there seem to be two competing processes: the immediate increase in conductivity in areas which were going through IRE and, on the other hand, a decrease in conductivity, which is slightly delayed, in areas where mostly reversible electroporation occurred. Brighter regions, which represent an increase in conductivity, would be associated with immediate irreversible electroporation whereas darker areas, which represent a decrease in conductivity, would be associated with partial permeabilization of the membranes that leads to cell swelling without immediate destruction of the membrane. Therefore, the overall effect of electroporation on tissue conductivity is not a simple linear relation where higher conductivity represents more membrane permeability.

It must be noted that decreased conductivity does not necessarily suggest that the cells in that region will survive. The decrease in conductivity indicates that the membrane was not completely destroyed, but it also indicates that water rushed into the cell and that cell homeostasis was compromised. Thus, the cell may eventually go through apoptosis and die nonetheless. This could justify the fact that, when we draw a graph equivalent to that of figure 7 but using the darker regions at 3 min after electroporation instead of the bright regions immediately after electroporation, the correlation between the actual damaged area and the estimated area was similar to the one obtained in figure 7.

Finally, the differences in the results from the three cases of 500 V pulses deserve further discussion. The conductance measurements, as taken from the electroporation electrodes during the pulses, in all three tests were similar (figure 9). So relying on these data for monitoring the electroporation process would not have been successful. As a matter of fact, the conductance (and its increase) for rat 7 is significantly higher than that of rat 8 and this should indicate a larger electroporation effect. On the other hand, the EIT measurements reveal the actual difference between the procedures in rats 7 and 9 and that of rat 8: liver of rat 8 is much more affected by the 500 V pulses than livers of rats 7 and 9. There could be several explanations for such differences but these are beside the point here. This is an example of the importance of monitoring the tissue impedance rather than measuring the electroporation pulse parameters.

We have shown that tissue impedance may be used as an indicator of tissue viability, but in a complex and intricate manner. Apart from the nonlinear transformation function between cell viability values and impedance measurements, there are also difficulties in measuring the impedance of each small region of the tissue. The EIT method is limited in terms of resolution for example, due in part to the use of regularization matrices. These are often applied to overcome the difficulty in solving the mathematically ill-posed problem of determining conductivity from boundary voltage measurements. The fact that the EIT electrodes in this case are quite close to the electroporation region suggests that minimally invasive EIT imaging may be clinically useful. This method would not rely on electrodes that are outside the body, but rather on a set of miniature electrodes that are inserted into the treated region. Some of the electrodes may be used for IRE, some for EIT and perhaps some for both. The results in the previous section show that although the reconstructed conductivity image is not a simple linear function of the electroporated region, such minimally invasive EIT may provide reliable feedback during an IRE procedure.

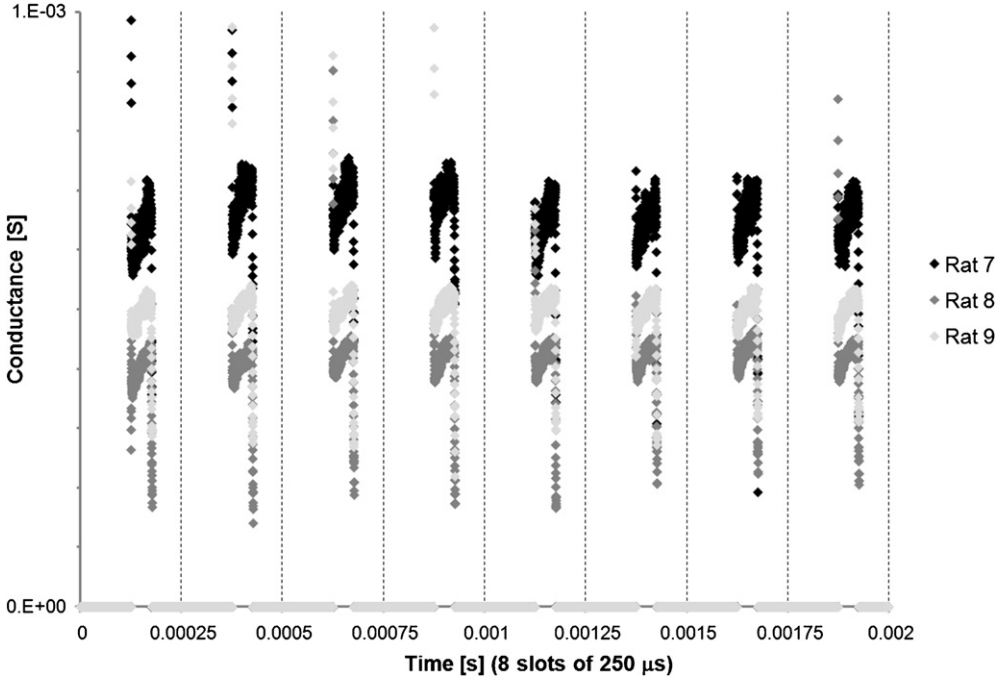

Figure 9. Conductance in rats 7, 8 and 9 measured during the application of the pulses.

5. Conclusions

EIT can indeed be employed to visualize the rapid tissue conductivity changes that occur during the application of electroporation pulses. We have obtained a reasonable correlation between the total area of regions with higher conductivity, as assessed immediately after the pulses, and the actual damaged area, as assessed by histological examination. Such correlation indicates that EIT is a valid method for monitoring electroporation treatments and that it could be employed in a closed-loop scheme.

Acknowledgments

This work was supported in part by the US National Institutes of Health (NIH) under Grant NIH R01 RR018961. B R has a financial interest in Excellin Life Sciences and is a consultant to AngioDynamics which are companies in the fields of electroporation, and he may gain financial benefit from this paper.

References

Abidor I G, Li L H and Hui S W 1994 Studies of cell pellets: II. Osmotic properties, electroporation, and related phenomena: membrane interactions *Biophys. J.* **67** 427–35

Adler A and Lionheart W R 2006 Uses and abuses of EIDORS: an extensible software base for EIT *Physiol. Meas.* **27** S25–42

Bayford R H 2006 Bioimpedance tomography (electrical impedance tomography) *Annu. Rev. Biomed. Eng.* **8** 63–91

Bertemes-Filho P, Brown B H and Wilson A J 2000 A comparison of modified Howland circuits as generators with current mirror type circuits *Physiol. Meas.* **21** 1–6

Canatella P J, Karr J F, Petros J A and Prausnitz M R 2001 Quantitative study of electroporation-mediated molecular uptake and cell viability *Biophys. J.* **80** 755–64

Chen C, Evans J A, Robinson M P, Smye S W and Toole P O 2008 Measurement of the efficiency of cell membrane electroporation using pulsed ac fields *Phys. Med. Biol.* **53** 4747–57

Cukjati D, Batiuskaite D, Andre F, Miklavcic D and Mir L M 2007 Real time electroporation control for accurate and safe *in vivo* non-viral gene therapy *Bioelectrochemistry* **70** 501–7

Davalos R V, Mir L M and Rubinsky B 2005 Tissue ablation with irreversible electroporation *Annu. Biomed. Eng.* **V33** 223–31

Davalos R V, Otten D M, Mir L M and Rubinsky B 2004 Electrical impedance tomography for imaging tissue electroporation *IEEE Trans. Biomed. Eng.* **51** 761–7

Davalos R V, Rubinsky B and Otten D M 2002 A feasibility study for electrical impedance tomography as a means to monitor tissue electroporation for molecular medicine *IEEE Trans. Biomed. Eng.* **49** 400–3

Edd J, Horowitz L, Davalos R V, Mir L M and Rubinsky B 2006 *In-vivo* results of a new focal tissue ablation technique: irreversible electroporation *IEEE Trans. Biomed. Eng.* **53** 1409–15

Edd J F and Davalos R V 2007 Mathematical modeling of irreversible electroporation for treatment planning *Technol. Cancer Res. Treat.* **6** 275–86

Esser A T, Smith K C, Gowrishankar T R and Weaver J C 2007 Towards solid tumor treatment by irreversible electroporation: intrinsic redistribution of fields and currents in tissue *Technol. Cancer Res. Treat.* **6** 261–74

Geddes L A 1972 *Electrodes and the Measurement of Bioelectric Events* (New York: Wiley-Interscience)

Gehl J and Mir L M 1999 Determination of optimal parameters for *in vivo* gene transfer by electroporation, using a rapid *in vivo* test for cell permeabilization *Biochem. Biophys. Res. Commun.* **261** 377–80

Granot Y and Rubinsky B 2007 Methods of optimization of electrical impedance tomography for imaging tissue electroporation *Physiol. Meas.* **28** 1135–47

Hofmann G A 2000 Instrumentation and electrodes for *in vivo* electroporation *Electrochemotherapy, Electrogenetherapy and Transdermal Drug Delivery: Electrically Mediated Delivery of Molecules to Cells* ed M J Jaroszeski, R Heller and R A Gilbert (Totowa, NJ: Humana Press) pp 37–61

Ivorra A and Rubinsky B 2007 *In vivo* electrical impedance measurements during and after electroporation of rat liver *Bioelectrochemistry* **70** 287–95

Jossinet J, Marry E and Matias A 2002 Electrical impedance endotomography *Phys. Med. Biol.* **47** 2189–202

Lee E W, Loh C T and Kee S T 2007 Imaging guided percutaneous irreversible electroporation: ultrasound and immunohistological correlation *Technol. Cancer Res. Treat.* **6** 287–94

Lionheart W R 2004 EIT reconstruction algorithms: pitfalls, challenges and recent developments *Physiol. Meas.* **25** 125–42

Maor E, Ivorra A, Leor J and Rubinsky B 2008 Irreversible electroporation attenuates neointimal formation after angioplasty *IEEE Trans. Biomed. Eng.* **55** 2268–74

Metherall P, Barber D C, Smallwood R H and Brown B H 1996 Three-dimensional electrical impedance tomography *Nature* **380** 509–12

Miklavcic D, Beravs K, Semrov D, Cemazar M, Demsar F and Sersa G 1998 The importance of electric field distribution for effective *in vivo* electroporation of tissues *Biophys. J.* **74** 2152–8

Mir L M, Belehradek M, Domenge C, Orlowski S, Poddevin B, Belehradek J J, Schwaab G, Luboinski B and Paoletti C 1991 Electrochemotherapy, a new antitumor treatment: first clinical trial *C. R. Acad. Sci., Paris* III **313** 613–8

Patterson R P 2005 Electrical Impedance Tomography: Methods, History, and Applications (Institute of Physics Medical Physics Series) *Phys. Med. Biol.* **50** 2427–8

Pavlin M, Kanduser M, Rebersek M, Pucihar G, Hart F X, Magjarevic R and Miklavcic D 2005 Effect of cell electroporation on the conductivity of a cell suspension *Biophys. J.* **88** 4378–90

Polydorides N and Lionheart W R B 2002 A Matlab toolkit for three-dimensional electrical impedance tomography: a contribution to the Electrical Impedance and Diffuse Optical Reconstruction Software project *Meas. Sci. Technol.* **13** 1871–83

Pucihar G, Mir L M and Miklavcic D 2002 The effect of pulse repetition frequency on the uptake into electropermeabilized cells *in vitro* with possible applications in electrochemotherapy *Bioelectrochemistry* **57** 167–72

Rigaud B, Morucci J P and Chauveau N 1996 Bioelectrical impedance techniques in medicine: I. Bioimpedance measurement. Second section: impedance spectrometry *Crit. Rev. Biomed. Eng.* **24** 257–351

Roberts M J 2004 *Signals and Systems: Analysis Using Transform Methods and MATLAB* (New York:: McGraw-Hill)

Rubinsky B 2007 Irreversible electroporation in medicine *Technol. Cancer Res. Treat.* **6** 255–60

Rubinsky B, Onik G and Mikus P 2007 Irreversible electroporation: a new ablation modality—clinical implications *Technol. Cancer Res. Treat.* **6** 37–48

Saulnier G J 2005 EIT instrumentation *Electrical Impedance Tomography: Methods, History and Applications* ed D S Holder (Bristol: Institute of Physics Publishing) pp 65–104

Weaver J C and Chizmadzhev Y A 2007 Electroporation *Biological and Medical Aspects of Electromagnetic Fields* ed F Barnes and B Greenebaum (Boca Raton, FL: CRC Press) pp 293–332

Wilson A J, Milnes P, Waterworth A R, Smallwood R H and Brown B H 2001 Mk3.5: a modular, multi-frequency successor to the Mk3a EIS/EIT system *Physiol. Meas.* **22** 49–54